A central function for perlecan in skeletal muscle and cardiovascular development

Jason J. Zoeller,[1,2] Angela McQuillan,[1,2] John Whitelock,[5] Shiu-Ying Ho,[3,4] and Renato V. Iozzo[1,2]

[1]Department of Pathology, Anatomy, and Cell Biology, [2]Cancer Cell Biology and Signaling Program, [3]Department of Biochemistry and Molecular Biology, and [4]Kimmel Cancer Center, Thomas Jefferson University, Philadelphia, PA 19107
[5]Graduate School of Biomedical Engineering, University of New South Wales, Sydney 2052, Australia

Perlecan's developmental functions are difficult to dissect in placental animals because perlecan disruption is embryonic lethal. In contrast to mammals, cardiovascular function is not essential for early zebrafish development because the embryos obtain adequate oxygen by diffusion. In this study, we use targeted protein depletion coupled with protein-based rescue experiments to investigate the involvement of perlecan and its C-terminal domain V/endorepellin in zebrafish development. The *perlecan* morphants show a severe myopathy characterized by abnormal actin filament orientation and disorganized sarcomeres, suggesting an involvement of perlecan in myopathies. In the *perlecan* morphants, primary intersegmental vessel sprouts, which develop through angiogenesis, fail to extend and show reduced protrusive activity. Live video-microscopy confirms the abnormal swimming pattern caused by the myopathy and anomalous head and trunk vessel circulation. The phenotype is partially rescued by microinjection of human perlecan or endorepellin. These findings indicate that perlecan is essential for the integrity of somitic muscle and developmental angiogenesis and that endorepellin mediates most of these biological activities.

Introduction

Heparan sulfate proteoglycans (HSPGs) comprise a complex and heterogeneous family of macromolecules that are preferentially located at the cell surface and basement membrane (Whitelock and Iozzo, 2005; Knox and Whitelock, 2006; Bishop et al., 2007). Perlecan, an archetypal HSPG with a large multivalent protein core, regulates basement membrane assembly, vascular and cartilage development, and tumor growth and angiogenesis (Mathiak et al., 1997; Iozzo, 1998; Iozzo and San Antonio, 2001; Hassell et al., 2002). The biology of perlecan extends far beyond the original notion as an anionic filter. This complex molecule has a variety of roles: perlecan is a structural constituent of basement membranes and is a key regulator of several growth factor signaling pathways and lipid metabolism (Fuki et al., 2000; Iozzo, 2005; Lindner et al., 2007). Moreover, although as a parent molecule, perlecan is proangiogenic (Aviezer et al., 1994; Sharma et al., 1998; Iozzo and San Antonio, 2001), a C-terminal perlecan fragment named endorepellin has antiangiogenic activity in tumor xenograft models (Mongiat et al., 2003; Bix et al., 2004, 2006; Woodall et al., 2008). Proteomic profiling of endorepellin-targeted action on the endothelium has recently identified five key proteins involved with endorepellin angiostatic activity (Zoeller and Iozzo, 2008).

The multiple developmental roles of perlecan are difficult to dissect in placental animals because disruption of the perlecan gene leads to embryonic lethality (Arikawa-Hirasawa et al., 1999; Costell et al., 1999). Nearly half of the perlecan-null mice die at embryonic days 10–12 because of hemorrhage within the pericardial cavity (Costell et al., 1999). The animals that survive exhibit severe cephalic and cartilage abnormalities and die of respiratory failure just after birth (Arikawa-Hirasawa et al., 1999). The phenotype of perlecan-null animals is quite complex in so far as a close analysis of all of the embryos that reach later stages of development show malformations of the cardiac outflow tract, including transposition of the great vessels and abnormal coronary artery development (Costell et al., 2002; González-Iriarte et al., 2003). A viable mutant animal has been generated in which mice lack perlecan exon 3, which contains two of the three possible heparan sulfate attachment sites (Rossi et al., 2003). Interestingly, the animals are viable and fertile but have small eyes and show degeneration of the lens within 3 wk of birth (Rossi et al., 2003). Various experimental challenges of

Correspondence to Renato V. Iozzo: iozzo@mail.jci.tju.edu

Abbreviations used in this paper: AChE, acetylcholine esterase; AChR, acetylcholine receptor; DA, dorsal aorta; DIC, differential interference contrast; DLAV, dorsal longitudinal anastomotic vessel; dpf, days postfertilization; hpf, hours postfertilization; HSPG, heparan sulfate proteoglycan; ISH, in situ hybridization; ISV, intersegmental vessel; PCV, posterior cardinal vein; SIV, subintestinal vessel.

The online version of this article contains supplemental material.

The Journal of Cell Biology, Vol. 181, No. 2, April 21, 2008 381–394
http://www.jcb.org/cgi/doi/10.1083/jcb.200708022

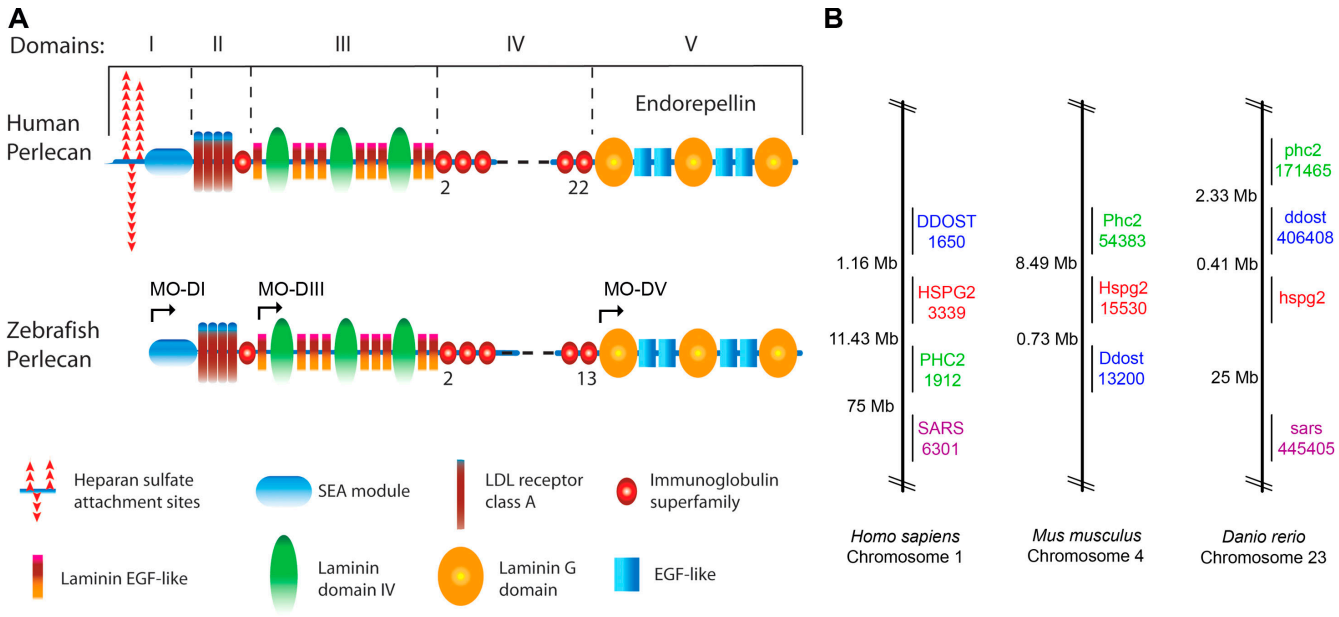

Figure 1. **Analysis of zebrafish *perlecan*.** (A) Schematic of human and zebrafish *perlecan* protein core. The roman numerals indicate the five domains. A key for the various modules is presented at the bottom. Arrows indicate the perlecan MO-DI, MO-DIII, and MO-DV morpholino targeting sites. See Fig. S1 for additional information (available at http://www.jcb.org/cgi/content/full/jcb.200708022/DC1). (B) Zebrafish perlecan is conserved syntenically. The zebrafish *perlecan* gene (*hspg2*) maintains a syntenic relationship with DDOST, PHC2, and SARS of mammalian species. Species and respective chromosome number are depicted; gene symbols are followed by the gene identification numbers from the National Center for Biotechnology Information Entrez Gene database, and distances between genes are displayed in megabases.

these heparan sulfate–deficient mice result in increased stenosis in injured carotid arteries (Tran et al., 2004) and impaired angiogenesis and tumor growth (Zhou et al., 2004).

In contrast to mammals, intact cardiovascular function is not essential for early zebrafish development because the embryos obtain adequate oxygen by simple diffusion from the environment. Morpholino-modified antisense knockdown of the *perlecan* gene allows the morphant embryos to survive for days essentially half-way through early larval development (~7 d postfertilization [dpf]), thereby permitting, for the first time, a detailed analysis of the role of perlecan in various systems during early and late embryogenesis.

In this study, we focused on the role of perlecan in zebrafish muscle and cardiovascular development. The *perlecan* morphants showed a severe myopathy characterized by abnormal fiber orientation, reduced amounts of actin filaments, and disorganized sarcomeres, suggesting a potential role for perlecan in human myopathies. Moreover, primary intersegmental vessel (ISV) sprouts initiated but did not completely extend and showed reduced protrusive activity; often the sprouts were very thin and blunt ended and either failed to anastomose or formed irregular junctions. Live videomicroscopy confirmed both the abnormal swimming motion caused by the muscular defects and the anomalous circulation in the head and trunk vessels. The morphant phenotype could be partially rescued by microinjection of human perlecan isolated from endothelial cells or by its C-terminal domain V/endorepellin. Collectively, our findings indicate that perlecan is essential for the development and integrity of somitic muscle and developmental angiogenesis and that its C-terminal module endorepellin mediates most of these biological activities.

Results

Cloning and developmental expression of zebrafish *perlecan*

We characterized the zebrafish *perlecan* sequence by electronic PCR and cloned zebrafish *endorepellin* by RT-PCR (TPA BK006379). From a comprehensive database analysis, we conclude that zebrafish perlecan has an overall structure similar to the mammalian counterpart with an estimated M_r of ~370 kD (Fig. 1 A) and good conservation of domains II–V (Tables S1 and S2, available at http://www.jcb.org/cgi/content/full/jcb.200708022/DC1). Notably, zebrafish *perlecan* lacked the first 56 amino acid residues and did not contain the SGD triplets present in the mammalian counterpart where the heparan sulfate chains are attached. However, there are 14 SG dipeptides dispersed throughout domains III–V (Table S2), with several of those conforming to the glycosaminoglycan-binding consensus found in other HSPGs (Bishop et al., 2007; Wang et al., 2007). Initial experiments showed that zebrafish *perlecan* is indeed an HSPG because it was completely resistant to chondroitinase ABC but was sensitive to heparitinase treatment (unpublished data). The exact domain in which the heparan sulfate chains are attached is not yet known. Moreover, nine Ig repeats were not present in zebrafish perlecan. Analysis of the available zebrafish database showed that there is one single gene encoding zebrafish *perlecan* and that it was localized to chromosome 23 syntenic to human chromosome 1 and mouse chromosome 4, where the mammalian orthologues are located (Fig. 1 B). Comparative analysis of human, mouse, zebrafish, and *Drosophila melanogaster* domain V/endorepellin showed a high degree of conservation with ~60% sequence identity and >70% homology between human and zebrafish endorepellin (Fig. S1 A).

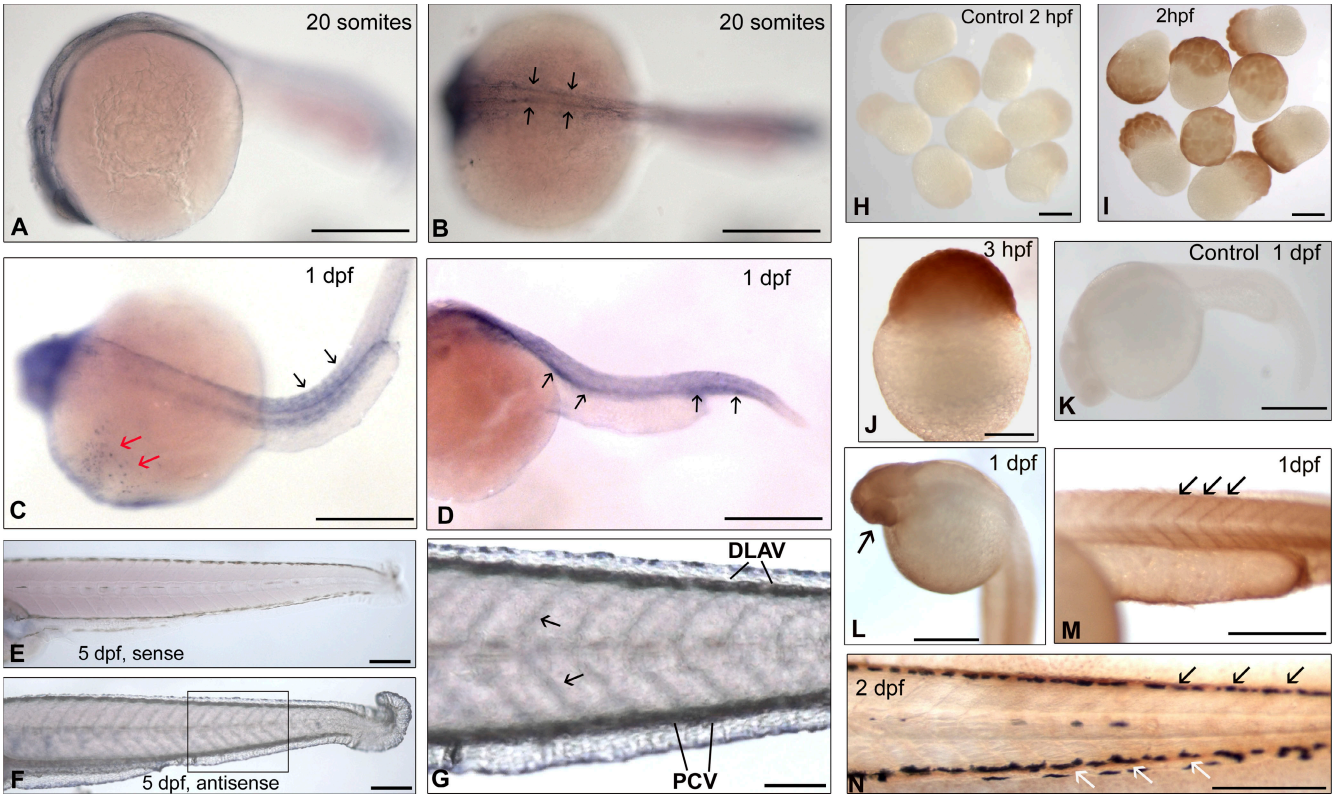

Figure 2. **Spatiotemporal expression patterns of zebrafish *perlecan* mRNA and protein.** (A–G) Whole mount ISH with a digoxigenin-labeled perlecan domain V antisense probe for the localization of *perlecan* mRNA (blue/purple staining). *Perlecan* mRNA can be detected at the 20-somite stage in regions of the developing brain (A) and along both sides of the notochord (B, arrows). At 1 dpf, *perlecan* expression is seen in the head region (C), in the developing somites (C, black arrows), and within the developing axial vasculature (D, arrows). Also note perlecan expression localized within the duct of Cuvier (C, red arrows). By 5 dpf (F and G [magnified image of the region boxed in F]), *perlecan* expression significantly increases throughout the trunk musculature (G, arrows), the major trunk/tail vessels including the DLAV, DA, and PCV, and in the developing gastrointestinal tract and future fin regions. (E) ISH with a digoxigenin-labeled perlecan domain V sense probe. ISH was performed in groups of two to five samples, and representative images are shown. (H–N) Whole mount immunohistochemistry with an affinity-purified anti–mouse perlecan antibody. Perlecan can be detected as early as the 64- and 1,000-cell stage of embryonic development (2 and 3 hpf, respectively) throughout the cell mound (I and J). At 1 dpf, perlecan protein (L and M) is detected throughout the head (L, arrow), trunk, and tail and is specifically localized to the developing muscle myoseptae (M, arrows) and the developing vasculature. By 2 dpf (N), perlecan protein is specifically detected in the trunk vasculature, including the DLAV (N, black arrows) and axial vessels (N, white arrows). (H and K) Immunohistochemistry images in which the primary antibody was omitted. Bars, 500 μm.

The BMP-1–sensitive site that would liberate the last globular domain of endorepellin, LG3, was perfectly conserved among human, mouse, and zebrafish, further stressing the potential biological significance of this protease-sensitive site (Gonzalez et al., 2005). Phylogenetic analysis of endorepellin from 13 separate species (Fig. S1 B) indicates that zebrafish and mammalian endorepellin evolved from a common ancestor.

To determine the spatiotemporal expression of zebrafish *perlecan*, we used whole mount in situ hybridization (ISH) and immunohistochemistry. ISH using a domain V antisense RNA probe showed the prominent expression of *perlecan* at the 20-somite stage in the head and somite region (Fig. 2, A and B). *Perlecan* was more clearly expressed at 1 dpf in these regions and was localized along the lateral myotomes (Fig. 2 C) and in the major axial vessels (Fig. 2 D). At 5 dpf, *perlecan* was expressed in the head and intestinal organs, with strong positivity in the axial vessels, including the dorsal aorta (DA) and the dorsal longitudinal anastomotic vessel (DLAV) as well as in the myoseptae, the ISVs, and posterior cardinal vein (PCV; Fig. 2, F and G).

Whole mount immunohistochemistry using an affinity-purified rabbit anti–mouse perlecan antibody (Handler et al., 1997) showed strong positivity at the 64- and 1,000-cell stage 2 and 3 h postfertilization (hpf; Fig. 2, I and J), at a time when zygotic transcription has not yet commenced, indicating that *perlecan* was maternally derived. At 1–2 dpf, perlecan epitopes were detected in the head region, in the developing eyes, along the myoseptae, and at the major axial vessels (Fig. 2, L–N), which is in agreement with the ISH results. The robust early embryonic expression of zebrafish *perlecan* indicates that this gene product is important for early embryogenesis.

Perlecan is essential for zebrafish embryonic development

To asses the developmental roles of perlecan, we selectively blocked the translation of *perlecan* mRNA using morpholino antisense oligonucleotides (MO), a specific translation inhibitor in zebrafish (Nasevicius and Ekker, 2000). We initially used two morpholinos of nonoverlapping sequence: one directed against the translation start site (MO-DI) of *perlecan* and the other encompassing the splice donor site of the initial exon of domain V/endorepellin (MO-DV; Fig. 1 A). Embryos at the one- to two-cell stage were injected with 2.5–10 ng morpholino, and embryos

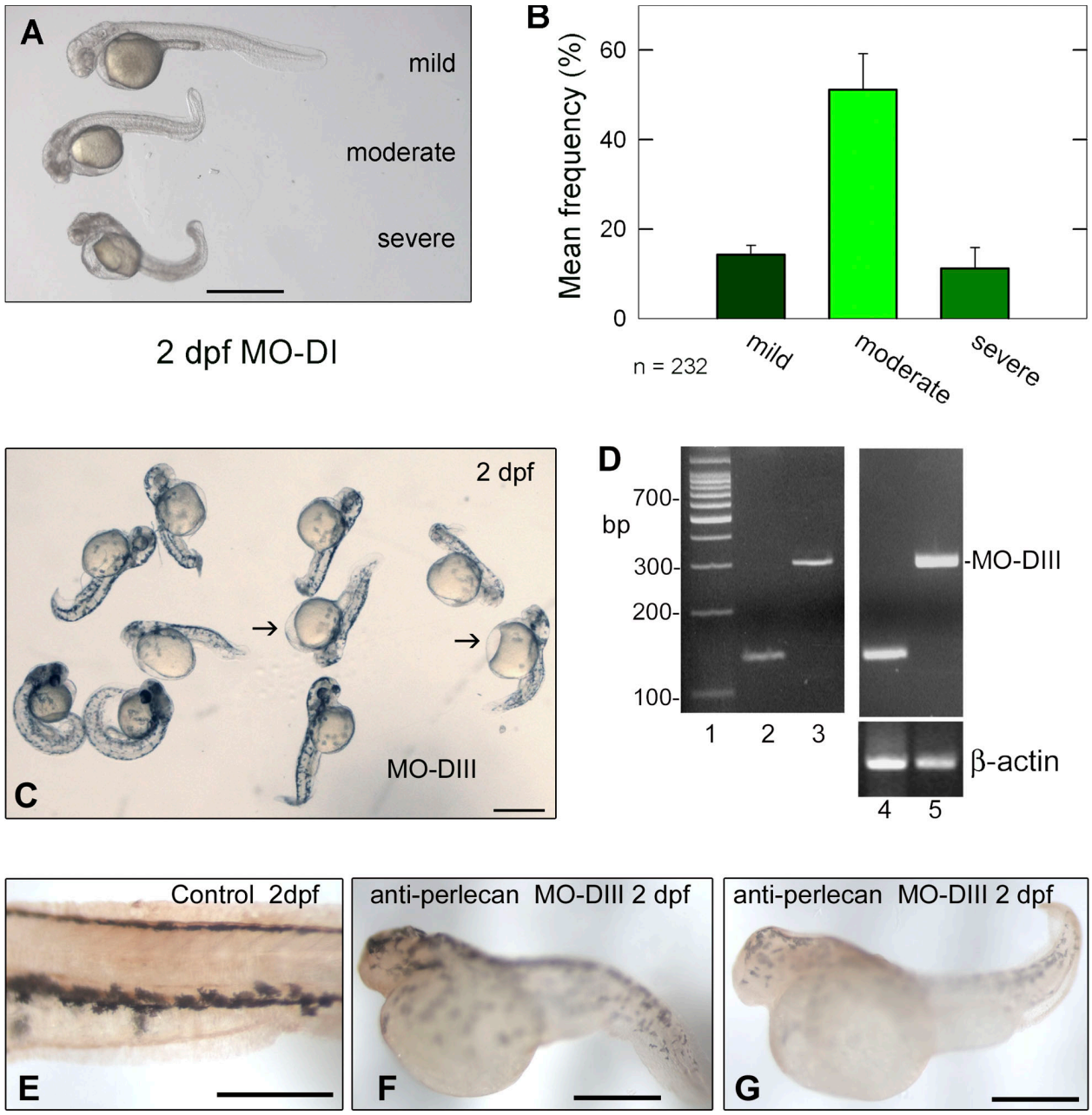

Figure 3. **Classification and verification of the *perlecan* morphant phenotype.** (A) All observed *perlecan* morphant phenotypes can be classified according to the degree of body twisting as presented for MO-DI. Categories include mild (least striking twisted body but noted tail phenotype), moderate (general twisted body usually accompanied by curly tail up), and severe (significant body plan shortening accompanied by twisting of the tail). (B) Mean observed frequencies of the twisted body classes from MO-DI *perlecan* morphant embryos (n = 232). Error bars represent ±SEM. (C) Phenotypic overview of perlecan splice junction–blocking MO-DIII. (D) RT-PCR verification of domain III splice junction–blocking morpholino effect. Note the band shift in morpholino-injected embryos (lane 5) versus uninjected embryos (lane 4), verifying the splice-blocking/intron retaining effect of MO-DIII. Lane 1, DNA ladder; lane 2, domain III PCR from zebrafish cDNA template; lane 3, domain III PCR from genomic DNA template; lane 4, domain III PCR from uninjected embryos' cDNA template; lane 5, domain III PCR from MO-DIII–injected embryos' cDNA template. The bottom bands in lanes 4 and 5 represent the β-actin control. Template from lanes 4 and 5 were derived from total RNA isolated from 23 embryos. See Fig. 1 A for additional details regarding the targeting positions of the morpholinos. (E–G) Whole mount immunohistochemistry for verification of domain III morpholino-based knockdown of *perlecan*. (E) Control uninjected embryo (2 dpf) shows perlecan expression throughout the trunk musculature and vasculature. (F and G) MO-DIII embryos (2 dpf) show significantly reduced perlecan protein levels in the trunk, with only minimal staining detected in the head and tail. A and E–G are left-side views with dorsal up and anterior to the left. Bars, 500 µm.

from the same matings were injected with an equal volume of phenol red/nuclease-free water mixture as a control. Higher morpholino concentrations (5–10 ng) caused significant lethality, especially for MO-DV; thus, we used 2.5 ng or less of the morpholinos. Both morpholinos produced an identical phenotype >90% (n = 358; $P < 0.001$; 10 independent experiments) with severe defects in the cardiovascular and musculoskeletal systems that became visible at 1 dpf (Fig. S2 A, available at http://www.jcb.org/cgi/content/full/jcb.200708022/DC1) and became progressively more apparent as development proceeded (Fig. S2, B–E). At 2 dpf, the morphants displayed a pronounced curvature of the tail and trunk, which could be classified as mild, moderate, or severe twisting of the

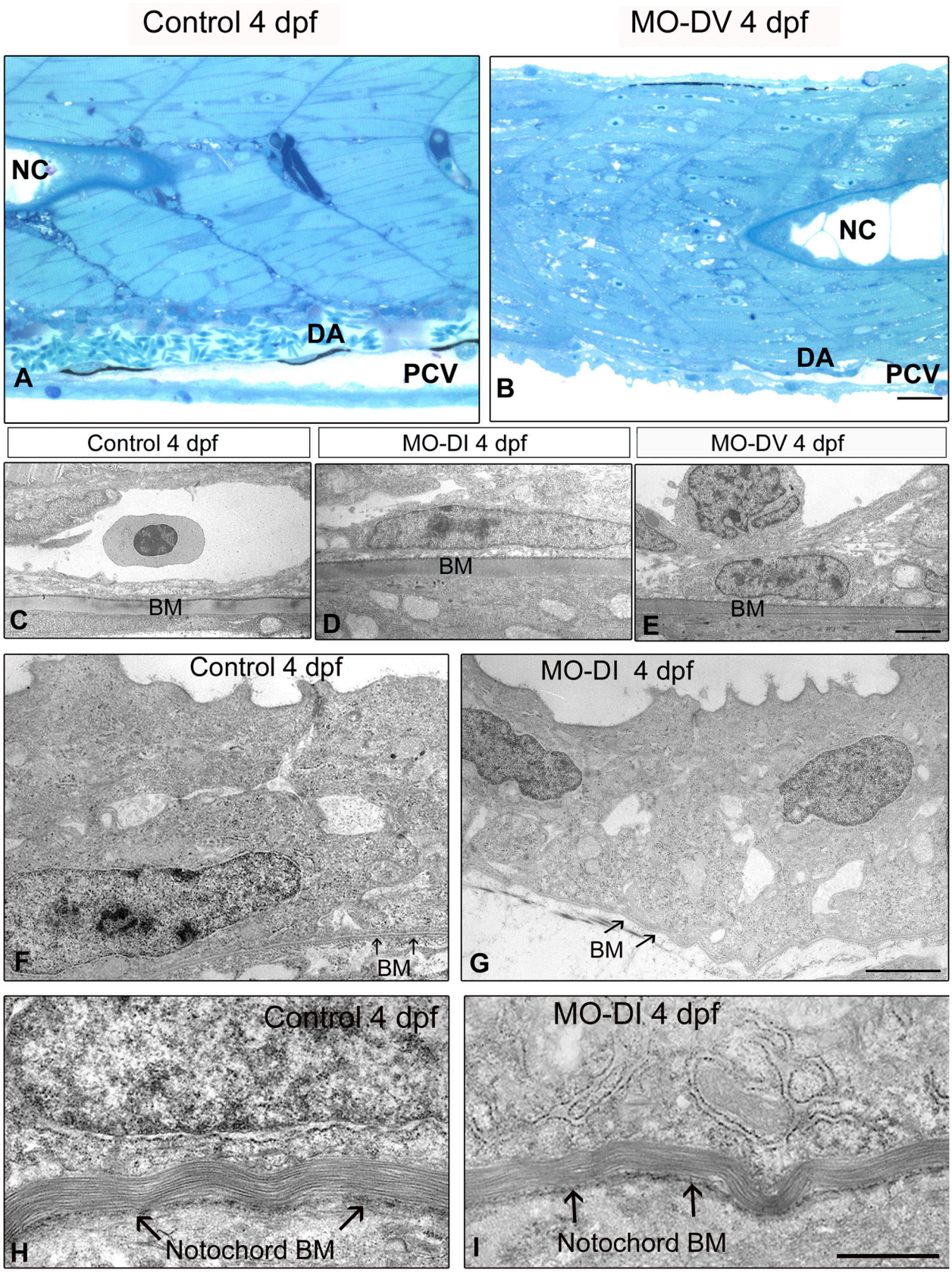

Figure 4. **Ultrastructural analysis of *perlecan* morphant embryos.** (A and B) Parasagittal epon sections stained with toluidine blue from 4 dpf control (A) and MO-DV morphant embryos (B). Note the irregular structure and organization of the morphant's skeletal muscle and associated abnormal u-shaped myoseptal boundaries. The DA appears collapsed in the morphant and devoid of blood cells. NC, notochord; DA, dorsal aorta; PCV, posterior cardinal vein. (C–I) A comparison of morphant and control basement membrane structure. Electron microscopy of the vascular (C–E), epithelial (F and G), and notochord basement membranes (BM; H and I) suggest that morpholino-based perlecan knockdown does not compromise the integrity of the basement membrane. Bars: (A and B) 25 μm; (C–I) 1 μm.

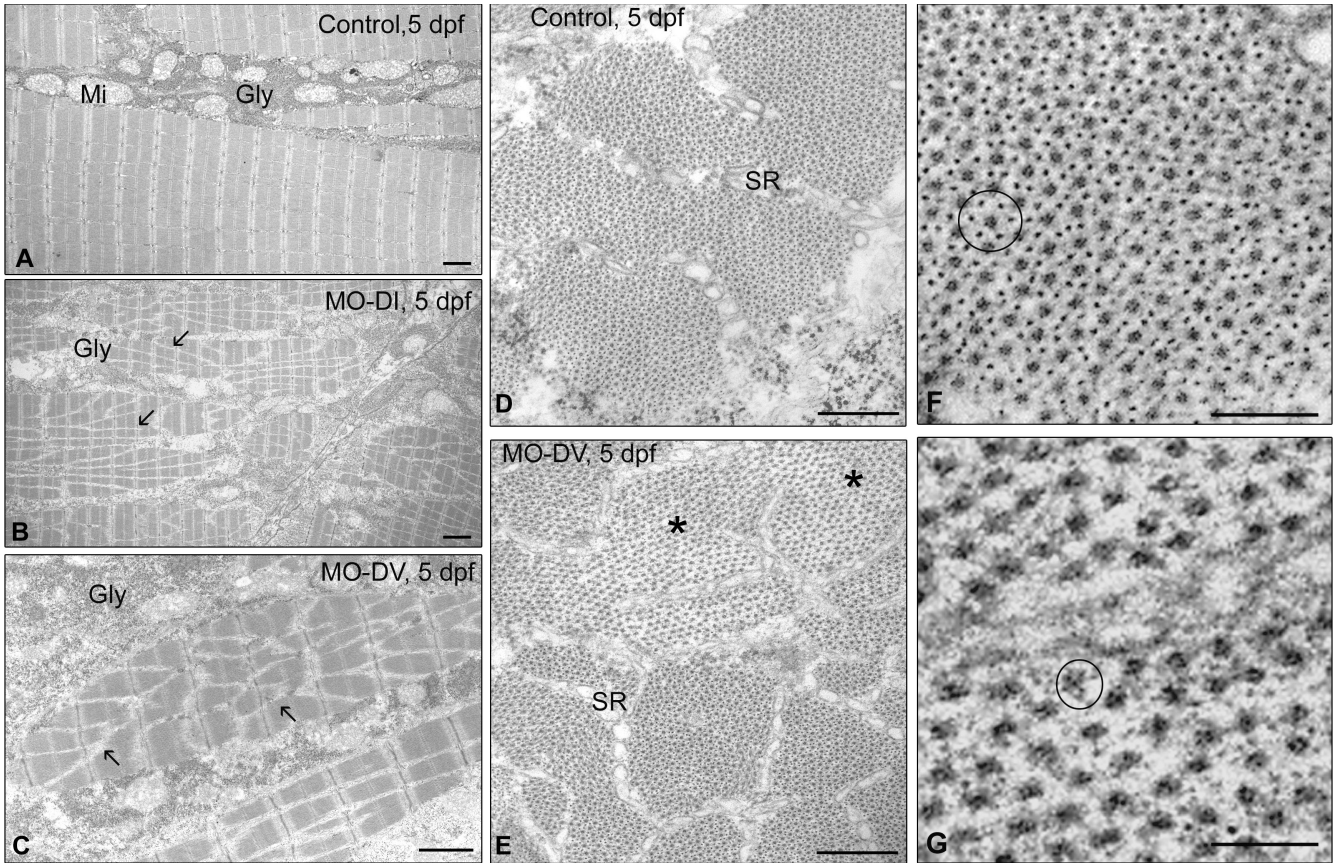

Figure 5. ***Perlecan* morphants display a complex muscular dystrophy phenotype.** (A, D, and F) Ultrastructural analysis of control skeletal muscle from a 5-dpf embryo. Parasagittal (A) and cross sections (D and F) of trunk muscle show typical muscular architecture with alignment of z bands, abundant glycogen (Gly) and mitochondria (Mi), and typical hexagonal arrays of thick and thin filaments (D). High magnification view shows thick filaments surrounded by six thin filaments (circle in F). In contrast, *perlecan* morphants induced by either translation-blocking (B) or splice-blocking (C, E, and G) morpholinos show disarray of muscular architecture with loss of filaments and irregular filaments traversing the sarcomeres at variable angles (arrows in B and C). Also notice the presence of areas with reduced thin filaments (asterisks in E) adjacent to more normal-appearing hexagonal structures (E). The sarcoplasmic reticulum (SR) appears to be normal (E). High magnification of the area labeled by the asterisk in E shows abnormal arrangement of thin and thick filaments (circle in G). Bars, 1 µm.

body (Fig. 3, A and B). The morphants exhibited either no escape response or uncoordinated movements in response to tactile stimuli and often swam in a circular fashion (Video 1).

To further corroborate the specificity of the morpholino-induced *perlecan* phenotype, we used an additional splicing-blocking morpholino-targeting domain III (MO-DIII; Fig. 1 A). The phenotype evoked by MO-DIII was identical to that evoked by MO-DI and MO-DV (Fig. 3 C). In five independent experiments ($n = 192$), MO-DIII injections caused a phenotype in 93 ± 5% of the injected embryos ($P < 0.001$). To establish that *perlecan* knockdown was responsible for the developmental anomalies, we purified total RNA from pooled control and MO-DIII–treated embryos ($n = 23$ for each group) and performed RT-PCR using two primers flanking the targeted exon of domain III. The predicted unprocessed RNA induced by MO-DIII would yield a band of ∼300 bp, whereas the processed RNA would yield a band of ∼150 bp. As positive controls, we used cDNA (Fig. 3 D, lane 2) and genomic DNA (Fig. 3 D, lane 3). MO-DIII completely abolished the properly processed *perlecan* mRNA as shown by the exclusive presence of the longer transcript of 300 bp (Fig. 3 D, lane 5) in contrast to the untreated embryos, which showed only the processed RNA band of 150 bp (Fig. 3 D, lane 4). In support of the specific perlecan knockdown, whole mount immunohistochemistry with the antiperlecan antibody showed a marked suppression of perlecan expression in the morphants (Fig. 3, F and G) as compared with controls (Fig. 3 E). The effects of the three morpholinos phenocopied each other, providing evidence that the observed developmental defects were specific for perlecan knockdown. The observed *perlecan* morphant's phenotype does not appear to be the result of developmental delay because we observed the onset of the heart beat and pigment development in all embryos. The morphants also exhibited a progressive dilatation of the pericardial sac in >90% of the cases. The embryos with the most severe phenotype survived 2–3 d, whereas the milder phenotype survived up to 7–9 dpf, at which time all of the morphants expired with severe generalized edema and cardiac failure, as shown by a progressive reduction in ventricular function and contractility.

To further prove the specificity of the observed *perlecan* knockdown phenotype, we performed two additional experiments in which we injected MO-DI and a morpholino targeting the p53 gene. The rationale for these studies is based on a recent report that morpholinos can nonspecifically activate the p53 gene, causing off-target phenotypic effects that are not caused by the specific morpholino used (Robu et al., 2007). In both experiments, the coinjection of MO-DI and p53 morpholino maintained the MO-DI

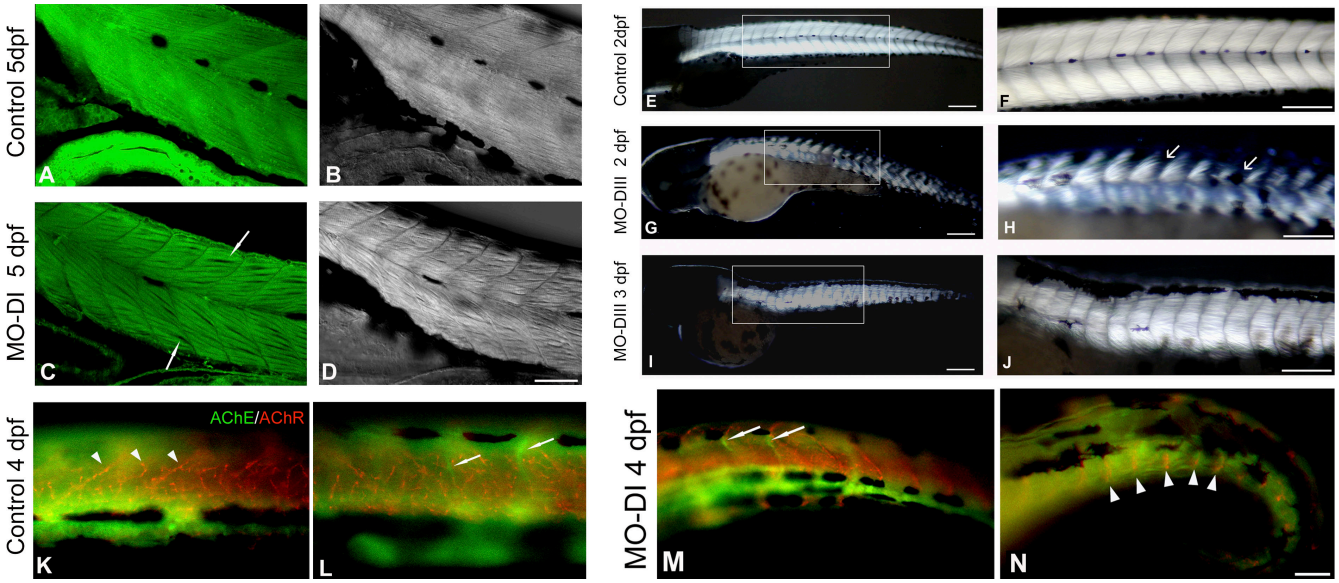

Figure 6. **Muscular analysis in *perlecan* morphant embryos.** (A and C) Filamentous actin confocal immunohistochemistry. Arows in C highlight clear spaces between the muscle fibers. (B and D) Corresponding DIC analysis of the trunk musculature from a control and morphant embryo at 5 dpf. (E–J) Birefringence analyses under polarizing light comparing control and morphant trunk muscle at 2–3 dpf. F, H, and J are magnified views of the boxed regions in E, G, and I, respectively. Arrows in H indicate regions of hypobirefringence. (K–N) Binding of fluorescently labeled α-bungarotoxin and fasciculin to 4-dpf control and morphant embryos as a means to examine the distribution of AChR (red; highlighted by arrowheads in K and N) and AChE (green; highlighted by arrows in L and M). Bars, 300 μm.

phenotype (Fig. S2 F), further confirming the specificity of MO-DI phenotypic effects. Any observed defects in head, brain, or eye development are likely nonspecific side effects of MO-DI morpholino because coknockdown with p53-MO did not maintain these phenotypic abnormalities. Additionally, a morpholino standard control oligonucleotide did not induce any phenotype (Fig. S2 F).

Perlecan is not required for the formation of most basement membranes

Longitudinal sections of the trunk of 4-dpf control zebrafish showed a well-formed DA filled with red cells and a properly developed PCV (Fig. 4 A). In contrast, in the *perlecan* morphants, the lumen of the DA was often collapsed and devoid of erythrocytes at 4 dpf (Fig. 4 B), although at earlier time points, the lumen was patent with circulation (see Perlecan is essential for developmental angiogenesis...). In addition, we observed a significant disruption of the muscular architecture in the *perlecan* morphants, with numerous vacuolizations and nucleated cells indicating muscle regeneration (Fig. 4 B). These lesions were found throughout the entire myotome, suggesting an essential role for perlecan in muscle development and maintenance. Ultrastructural analysis of various basement membranes, including vessels, skin, and notochord, showed no significant alterations in the morphants (Fig. 4, C–I), which is in agreement with the perlecan-null mice in which basement membrane assembly is developmentally normal (Arikawa-Hirasawa et al., 1999; Costell et al., 1999).

Loss of perlecan causes an unexpected severe myopathy

To understand the effects of *perlecan* knockdown on muscle patterning, we performed a detailed ultrastructural analysis of the control and morpholino-treated embryos. The muscular phenotype was evident at 2 dpf with significant loss of myofilaments and disruption of mitochondria (Fig. S3, available at http://www.jcb.org/cgi/content/full/jcb.200708022/DC1). However, the muscular phenotype became progressively more severe with time. By 5 dpf, control embryos exhibited a well-defined muscle structure, with highly organized bundles of myofibers surrounded by mitochondria and glycogen (Fig. 5 A). In contrast, morphants induced by either translation- or splice-blocking morpholinos showed a marked disarray of muscle fibers (Fig. 5, B and C). Often, the filaments appeared to be interwoven, and clear (less electron dense) bands traversed the sarcomeres at a longitudinal angle, whereas the I bands, the clear bands containing the thinner and darker Z bands, were often misaligned and tortuous (Fig. 5 C). In cross sections, control filaments were assembled in a hexagonal arrangement typical of mature myofibrils, with each thick filament (myosin filaments) encircled by six thin filaments of actin that are situated at the trigonal positions of the lattice so that each is shared by three equidistant thick filaments (Fig. 5, D and F). In the *perlecan* morphants, cross section analysis confirmed the misalignment and irregular ultrastructure observed in the longitudinal sections. Specifically, we found irregular hexagonal arrays and areas in which the thick filaments were not associated with thin filaments (Fig. 5 E). Because of the interwoven and twisted nature of the sarcomere, it was difficult to take focused electron micrographs, and, in the few exceptions, the thin filaments of actin were irregularly aligned with the thick myosin filaments (Fig. 5 G). Essentially, myofilaments were present but incorrectly oriented. However, the structure of the sarcoplasmic reticulum was fully preserved.

Next, we investigated the distribution of actin-containing filaments using fluorescently labeled phalloidin. The morphants

exhibited blocky somites, with less defined chevron-shaped boundaries and often clear spaces between the muscle fibers (Fig. 6 C, arrows). The muscle bundles were often interwoven, which is better illustrated under differential interference contrast (DIC) microscopy (Fig. 6 D), as compared with the regular array of muscle bundles in the control larvae (Fig. 6, A and B).

Examination of control embryos using polarized light microscopy, a technique used to investigate various muscle mutant zebrafish (Granato et al., 1996; Kunkel et al., 2006), revealed that axial muscle was highly birefringent at 2 dpf (Fig. 6, E and F) as a result of the ordered array of myofilaments in striated muscle. In contrast, *perlecan* morphants showed an overall decrease in birefringence with patchy areas of hypobirefringence, suggesting a severe disruption of the sarcomeric structures (Fig. 6, G and H). Moreover, in the morphants with a moderate phenotype, the chevron-shaped myoseptae were smooth and u shaped (Fig. 6, I and J).

Next, we studied the muscular expression of acetylcholine esterase (AChE) and its receptor (acetylcholine receptor [AChR]) in control and morphant embryos. The rationale for these studies is based on the fact that a set of molecules, including AChE, AChR, perlecan, and dystroglycan, cluster at the neuromuscular junction, where muscle contraction is initiated (Rotundo, 2003). The collagen-tailed form of AChE is highly expressed in the innervated regions of skeletal muscle fibers and is attached to the synaptic basement membrane. It has been shown that perlecan is essential for targeting of the collagen-tailed form of AChE to the neuromuscular junction (Arikawa-Hirasawa et al., 2002). We used whole mount zebrafish embryos at 4 dpf and two toxins, AlexaFluor488-labeled fasciculin (green) and AlexaFluor555-labeled α-bungarotoxin (red), to label AChE and AChR, respectively. In control zebrafish trunk, AChR was distributed as a fine array along the fibers and at myoseptal junctions (Fig. 6 K), whereas AChE labeling was diffuse with focal clustering at the myoseptal junctions (Fig. 6 L). The *perlecan* morphants displayed a marked reduction and mislocalization of AChR, and short clusters of AChE were detected at the myoseptal junctions, often with skipping of somites (Fig. 6 M). In the most severe morphants, AChR clustered to intersomitic septae (Fig. 6 N), with the somites mostly devoid of AChR.

Collectively, our findings indicate that perlecan is essential for the development and integrity of somitic muscle and suggest a relationship between AChR and perlecan. The lesions were found throughout the entire myotomes, demonstrating an essential role for perlecan in skeletal muscle development and maintenance. The loss and misalignment of myofilaments could potentially induce abnormal and uncoordinated movement. This could provide a plausible explanation for twisting of the body and tail and for the circular swimming observed in the *perlecan* morphants with severe phenotypes (Video 1).

Perlecan is essential for developmental angiogenesis and cardiovascular function

To monitor vascular development, we used two transgenic zebrafish expressing *gfp* under the guidance of either the *fli1* (Lawson and Weinstein, 2002) or *vegfr2* promoter (Cross et al., 2003). The transcription factor *fli1* and *vegfr2/flk1* are two endodermal vascular markers of vascular cell fate and specification (Carmeliet, 2005). Thus, in both transgenic fish, there is an endothelial-specific expression of *gfp*, thereby allowing continuous in vivo observation of vertebrate embryonic vascular development.

In contrast to the axial vessels, DA and PCV, the ISVs and parachordal vessels develop through angiogenesis (Childs et al., 2002). The ISVs are the primary sprouts emerging from the DA at ∼1 dpf. They are partially patent by 1.5 dpf and fully functional by 2 dpf (Isogai et al., 2003). The ISVs follow a pattern that is independent from circulation and is tightly regulated by spatially and temporally defined genetic cues (Childs et al., 2002; Isogai et al., 2003). As the growing ISVs approach the dorsolateral roof of the neural tube, they divide into two major branches that turn caudally and rostrally to form the DLAVs (Isogai et al., 2001, 2003). The secondary angiogenic sprouts emerge exclusively from the PCV and develop into the primary vascular network. The parachordal vessels, which are positioned along the horizontal myoseptae at either side of the notochord, arise by angiogenic growth of secondary sprouts from the PCV (Isogai et al., 2003). The *perlecan* morphants showed relatively well-developed axial vessels but exhibited significant suppression of ISVs as compared with control embryos (Fig. 7, A–D). At 2 dpf, the ISVs were only partially formed, and the DLAVs were not formed at all in the most severe phenotypes induced by the translation-blocking morpholino MO-DI. The sprouts exhibited a reduced protrusive activity and were very thin and blunt ended. The endothelial cells often did not completely migrate along the myoseptae from the DA (>90%; $n = 287$ in six separate experiments) and followed abnormal paths failing to interconnect. In most cases, the ISV stopped at the level of the notochord (Fig. 7, B and D) and failed to form the regular lattice of vessels present on either side of the trunk. At later stages, some ISV sprouts reached the DLAV level, but they did not properly assemble these vessels, and several misguided vessel branches were noted growing away from the vertical myoseptae (Fig. S4, available at http://www.jcb.org/cgi/content/full/jcb.200708022/DC1). The persistence of these anomalous vessels at 3–4 dpf indicates that the phenotype of the perlecan morphants is not the result of just a nonspecific developmental delay caused by the morpholino injection. Identical vascular changes were generated by the splice-blocking morpholino MO-DV ($n = 225$; six independent experiments; Fig. S5, A–H).

The *perlecan* morphants induced in the *vegfr2-gfp* transgenic zebrafish also produced an identical phenotype with a poorly formed angiogenic network (Fig. S5, I–N). In addition, there was pericardial edema and stretching of the atrium and ventricle, which became more severe with time (Fig. S5, K–N). Similar results were obtained with the splicing morpholinos MO-DV and MO-DIII (unpublished data). Overall, there was a concurrent reduction in heart beats per minute with a mean of 98 ± 8 for the morphants versus 158 ± 11 for the controls ($n = 24$; $P < 0.001$).

By live DIC videomicroscopy, we observed robust circulation in the control heart, head, and axial vessels as well as the various branches emanating from the DA, PCV, and DLAV (Videos 2 and 4, available at http://www.jcb.org/cgi/content/full/jcb.200708022/DC1). In contrast, in the most severe phenotype caused by the knockdown of *perlecan*, we observed no circulation in the head and trunk regions in spite of robust heart contraction (Video 3). In the milder morphant phenotype,

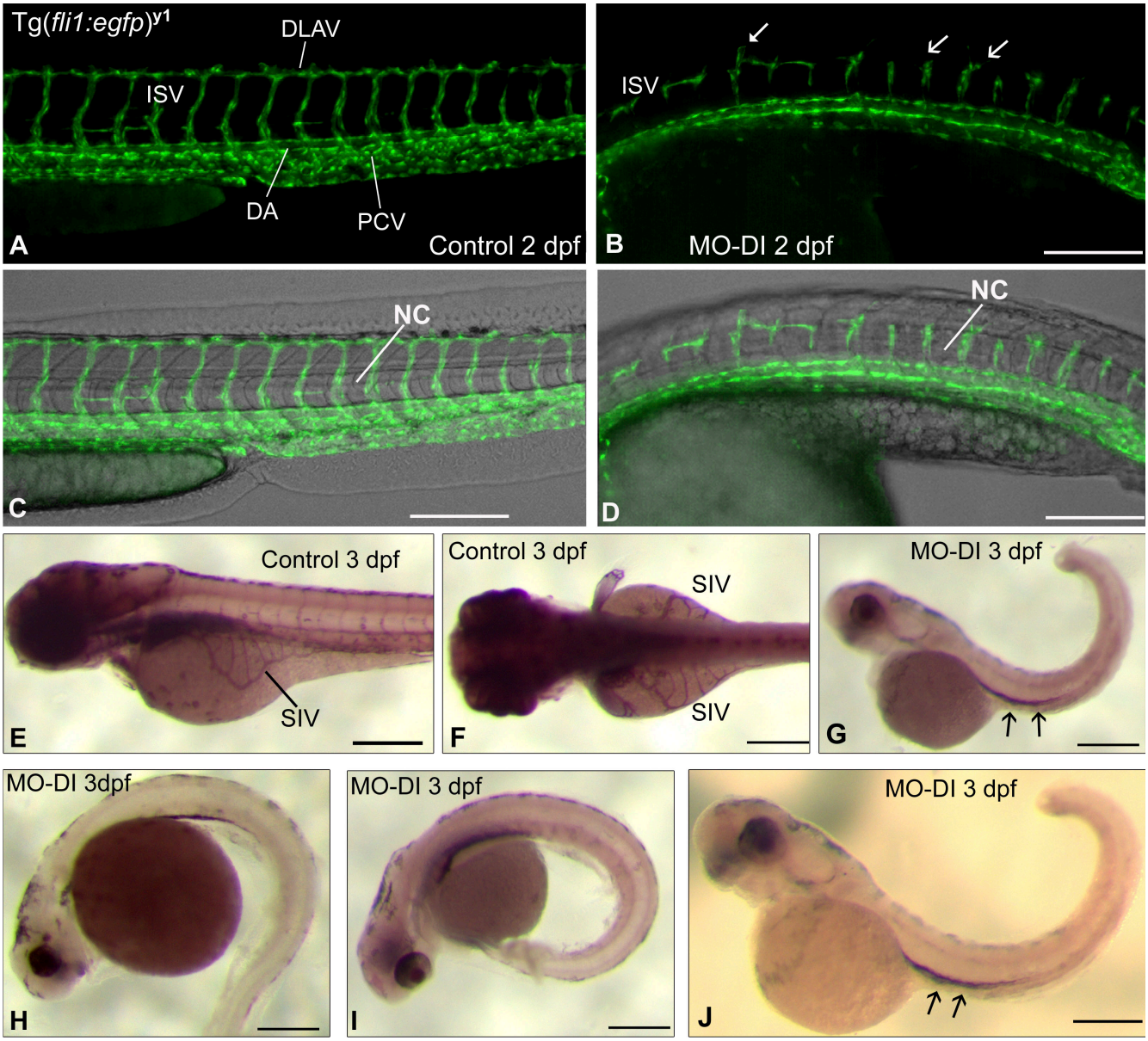

Figure 7. **Vascular analysis in *Tg(fli1:egfp)*^{y1} *perlecan* morphant embryos.** (A and B) Epifluorescence microscopy with 3D deconvolution comparing the trunk vasculature of 2-dpf control versus MO-DI embryos. Note the correct formation of DLAV, ISV, DA, and PCV in the control (A). In contrast, the *perlecan* morphant (B) exhibits abnormal ISVs. Often the ISV sprouts fail to completely migrate along the myoseptae and to anastomose (arrows). (C and D) Merged images corresponding to those shown in A and B taken with both fluorescence deconvolution and DIC microscopy. Note that the ISVs barely reach the notochord (NC) and do not properly migrate to the dorsal region, thereby failing to interconnect and properly form the DLAV. (E and F) Lateral and dorsal views of alkaline phosphatase–stained control embryos at 3 dpf. Notice the well-developed SIV. (G–I) Three representative MO-DI *perlecan* morphants showing the complete absence of SIV and reduced alkaline phosphatase staining throughout the trunk vasculature and head region. Notice that J is a higher magnification of G. The only detectable signal is present along the axial vessels (arrows in G and J). Bars, 500 μm.

we saw regular blood flow through the axial vessels but a greatly diminished or absent circulation in the ISVs and DLAVs (Videos 5 and 6). These results indicate that the disrupted or malformed ISVs and DLAVs are not functionally patent in the perlecan morphants.

Next, we examined endogenous alkaline phosphatase activity as a marker enzyme for the developing vasculature. In control embryos, the endogenous alkaline phosphatase activity labeled the major cerebral and axial vessels as well as the subintestinal vessels (SIVs), which develop by angiogenesis from the DA at ~3 dpf (Fig. 7, E and F). In contrast, all MO-DI morphants showed a marked reduction in alkaline phosphatase staining of the head and axial vessels and a total absence of SIV labeling (Fig. 7, G–J). The profound effects of *perlecan* knockdown on endothelial cell alkaline phosphatase activity suggests that the vascular changes are not secondary to abnormal somitic muscle development but are specific for endothelial cells, further proving the significant effects of *perlecan* deficiency on developmental angiogenesis. We conclude that *perlecan* is essential for both robust migration of the primary endothelial sprouts and for maintaining the path of these vessels along the vertical myoseptae.

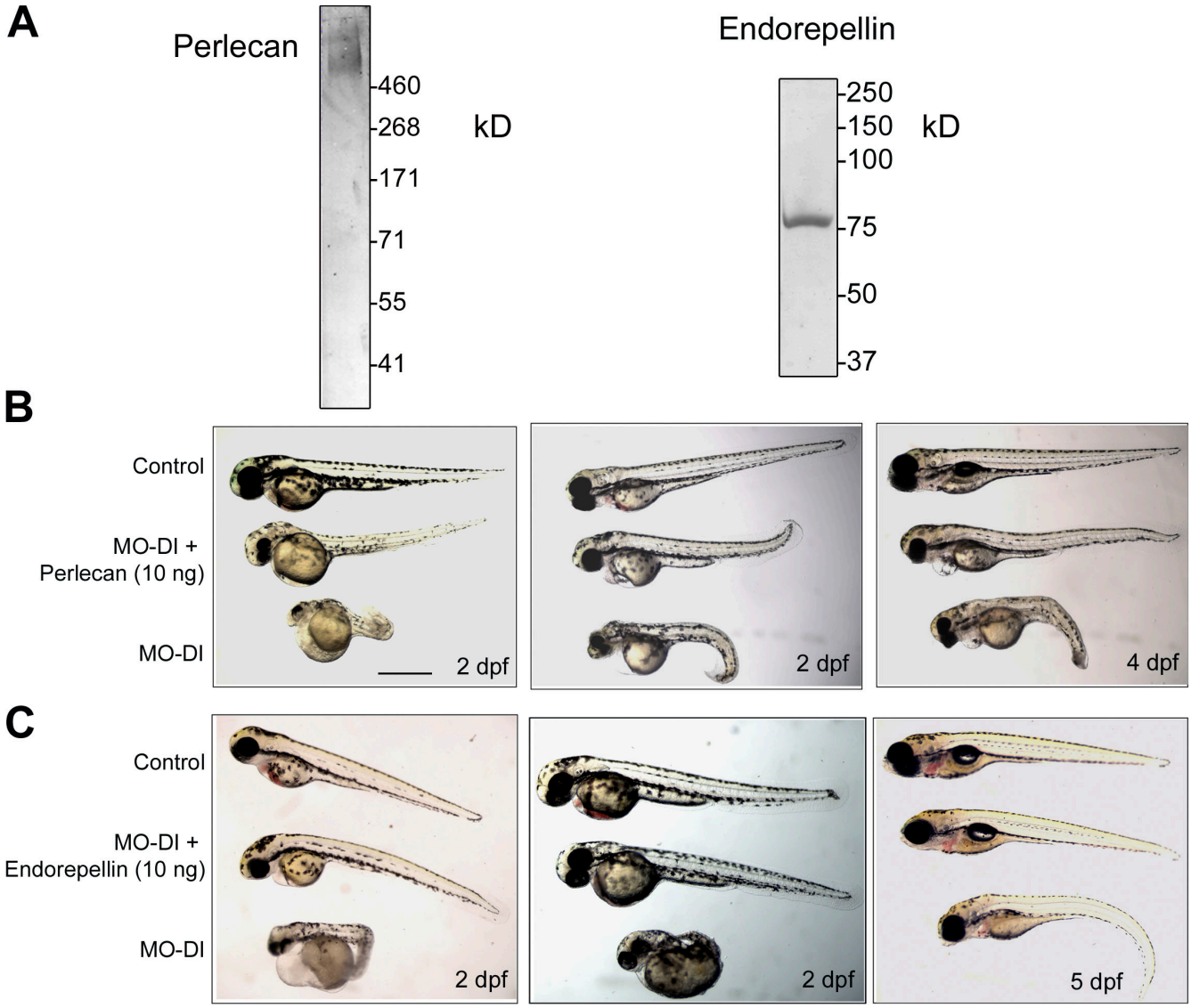

Figure 8. **Partial rescue of the perlecan morphants by human *perlecan* and endorepellin.** (A) Coomassie blue–stained 3–8% Tris-borate gradient gel of human perlecan immunopurified from human coronary artery endothelial cells (left). Note the large and broad band corresponding to M_r of >500 kD. The right panel shows a Coomassie blue–stained 10% SDS-PAGE of human endorepellin. (B and C) Composite photographs of control, MO-DI, and MO-DI coinjected with perlecan or endorepellin at the designated concentrations. The rescue phenotype was calculated based on the degree of body twisting as compared with the microinjection of MO-DI alone. Notice the partial rescue of the twisted body phenotype in both cases. Bar, 500 µm.

Rescue experiments using human perlecan and endorepellin

Conclusive determination of any phenotype is generally made through targeting of the same gene at several nonoverlapping sites using antisense morpholinos or by RNA/protein rescue. Given the large size of *perlecan* mRNA (predicted mRNA of ~12 kb), rescue of the morphant phenotype by the overexpression of cRNA encoding full-length zebrafish *perlecan* would be technically impractical. Because of the high degree of homology between human and zebrafish perlecan, we chose to inject human perlecan or endorepellin. The former was immunopurified from human coronary artery endothelial cells using an affinity column coupled with antiperlecan monoclonal antibody (Whitelock et al., 1999), whereas the latter was purified from the media conditioned by human embryonic kidney 293–Epstein-Barr virus nuclear antigen cells stably expressing domain V/endorepellin (Mongiat et al., 2003). The purity of the two preparations is shown in Fig. 8 A. Embryos were injected with 2.5 ng MO-DI and were randomized into two groups. Half of the embryos received phenol red, whereas the other half received 10 ng perlecan or domain V/endorepellin. A significant rescue of the twisted body phenotype (ranging between 66 and 82%; $n = 29$ for perlecan and $n = 36$ for endorepellin) was achieved by coinjection of full-length perlecan or endorepellin. The rescue of the phenotype was quite striking, and several zebrafish survived up to larval stage (Fig. 8, B and C). Notice that the effects of the morpholinos in the rescued morphants are still visible, including slightly bent tails and moderate pericardial edema (Fig. 8, B and C), indicating that perlecan and endorepellin were capable of rescuing the phenotype, at least partially. Collectively, these findings complement the immunohistochemical data, corroborate the specificity of our antisense strategy, and support a key role for perlecan and endorepellin in maintaining cardiovascular and musculoskeletal function.

Discussion

In this study, we used a targeted protein depletion approach coupled with protein-based rescue experiments to investigate the role of perlecan in vertebrate development. Perlecan exhibited novel and unique functions in muscle development and angiogenesis. Moreover, similar phenotypes were observed in three distinct genetic backgrounds, including wild type and two transgenic fish lines. The *perlecan* morphants showed a severe myopathy characterized by abnormal orientation and reduced amounts of actin filaments and disorganized sarcomeres. In the *perlecan* morphants, primary ISV sprouts initiated but did not completely extend and showed reduced protrusive activity. Essentially, vessels were severely constricted or atretic with reduced or absent functional circulation as clearly documented by live videomicroscopy. Thus, perlecan plays a central role in the complex process of angiogenesis by providing guidance for endothelial cell migration and differentiation as well as branching morphogenesis.

Unexpected role for perlecan in muscular development

In the mouse, perlecan is essential for localizing AChE to the neuromuscular junctions (Peng et al., 1998, 1999; Arikawa-Hirasawa et al., 2002; Rotundo, 2003). As the collagen-tailed form of AChE binds directly to perlecan and colocalizes with perlecan and AChR when transplanted onto frozen sections of muscle, it is likely that perlecan is a major acceptor site for AChE at the neuromuscular junctions (Arikawa-Hirasawa et al., 2002). This concept is further strengthened by the fact that perlecan binds to α-dystroglycan and that in the absence of α-dystroglycan, neither perlecan nor AChE accumulates at the neuromuscular junctions (Arikawa-Hirasawa et al., 2002). Moreover, the cell surface–binding LG domains of muscle agrin and perlecan promote AChR clustering in the presence of laminin-2 (Smirnov et al., 2005). The *perlecan* morphants displayed a marked reduction and mislocalization of AChR, and short clusters of AChE were noted at the myoseptal junctions, often with skipping of somites. In the most severe morphant phenotypes, AChR clustered in small regions corresponding to intersomitic septae, with the somites mostly devoid of AChR. We note that in zebrafish embryos and larvae, AChE is not clustered as in mammalians and is relatively diffuse in the trunk somites even though the synaptic currents in larvae appears to be mature (Drapeau et al., 2001). The lesions were found throughout the entire myotomes, demonstrating an essential role for perlecan in skeletal muscle development and maintenance. The severity and progressive myopathy caused by perlecan deficiency may be partly caused by the fact that zebrafish embryonic muscle may not possess the regenerative capacity of mammalian muscle (for review see Bassett and Currie, 2003).

The loss and misalignment of myofilaments could potentially induce abnormal and uncoordinated movement, a plausible explanation for twisting of the body and tail and for the circular swimming. These findings indicate that perlecan is essential for the development and integrity of somitic muscle and suggest a relationship between AChR and perlecan. Notably, a zebrafish null mutation in AChE (*ache*; Behra et al., 2002) shows a muscular phenotype similar to that of the *perlecan* morphants, further stressing the role of AChE in generation of the myopathy.

The muscular phenotype evoked by blocking *perlecan* expression is similar to that observed in the *sapje* mutant, in which expression of the zebrafish orthologue of the X-linked human Duchenne muscular dystrophy, dystrophin, is absent (Bassett et al., 2003). The overall loss of myofilaments and muscle architecture of the *sapje* mutant is similar to the ultrastructural appearance of the *perlecan* morphant skeletal muscle (see Fig. 6 C of Bassett et al., 2003). In the *sapje* mutants, however, the sarcomeres often collapse as a result of their detachment from the myoseptae, a process that leads to enhanced fiber death. We did not detect any clear muscle detachment in the *perlecan* morphants, suggesting that other factors are involved in this process.

The absence of dystrophin caused by either a mutation in exon 4 of the dystrophin gene in *sapje* mutants (Bassett et al., 2003) or by antisense morpholino (Guyon et al., 2007) leads to destabilization of the dystrophin-associated protein complex analogous to what is observed in mammals. A similar muscular phenotype was observed by knockdown of other members of the dystrophin-associated protein complex, including dystroglycan (Parsons et al., 2002) and δ-sarcoglycan (Guyon et al., 2005). Domain V/endorepellin binds with high affinity to α-dystroglycan (Talts et al., 1999), and posttranslational or genetic disruption of dystroglycan function also disrupts perlecan binding to dystroglycan (Kanagawa et al., 2005). Moreover, perlecan and dystroglycan act at the basal side of the *Drosophila* follicular epithelium to maintain epithelial organization (Schneider et al., 2006). Collectively, these data suggest that perlecan is a component of a trimolecular complex (laminin–perlecan–dystroglycan) whose disruption could be involved in the pathogenesis of glycosylation-deficient muscular dystrophy (Kanagawa et al., 2005). Domain V/endorepellin interacts with nidogen, fibulin-2, and collagens IV and XVIII in basement membranes (Iozzo, 2005; Knox and Whitelock, 2006), and interaction of skeletal muscle cells with collagen IV is mediated by cell surface–associated perlecan (Villar et al., 1999). Thus, *perlecan* reduction or absence during development could lead to abnormal cell matrix interactions.

Our findings indicate that perlecan might be directly involved in muscular dystrophy, and, although perlecan mutations have been implicated in causing Schwartz-Jampel syndrome characterized by myotonia and chondrodysplasia (Stum et al., 2006; Rodgers et al., 2007), a role for perlecan in the pathogenesis of muscular dystrophy has never been hypothesized before. It will be important to investigate perlecan mutations in humans, especially in patients lacking any mutation in established human causative genes.

A key role for *perlecan* in developmental angiogenesis and cardiovascular function

Anatomically, vascular development in zebrafish proceeds as in other vertebrates (Isogai et al., 2001, 2003; Childs et al., 2002; Lawson and Weinstein, 2002). The major axial vessels derive from angioblast migration from the lateral plate mesoderm, whereas secondary vessels form by angiogenesis shortly after coalescence of the angioblasts at the midline. Analogous to

perlecan knockdown, suppression of *Vegfa* by antisense morpholino (Nasevicius et al., 2000) or VEGF receptor blockade by the small molecule SU5416 (Cross et al., 2003) inhibits ISV formation and causes pericardial edema. These data suggest that the pathology caused by the knockdown of *perlecan* or VEGFA is caused by an aberrant vascular system rather than by nonspecific effects.

Using two transgenic lines of zebrafish expressing *gfp* driven by the promoter of *fli1*, an ETS domain transcription factor specific for cells of the hemangioblastic lineage, or *vegfr2/flk1*, the major receptor for VEGF, we showed that perlecan was not required for endothelial cell differentiation and vasculogenesis. However, *perlecan* knockdown caused a marked reduction in circulating blood cells in the most severe phenotypes, suggesting a potential role for *perlecan* in the establishment of angioblast differentiation and lineage. *Perlecan* morphants showed a marked impairment in the ability of *vegfr2/fli1*-expressing endothelial cells to migrate along the intersomitic septae and form arterio-venous channels. The live videomicroscopy analysis clearly showed a wide spectrum of vascular changes ranging from a reduced to a complete lack of circulatory cells in the ISV, DLAV, and SIV. Disruption of ISV and SIV by knockdown of *perlecan* is particularly interesting because these vessels develop by angiogenic sprouting, a process that closely resembles tumor angiogenesis. Notably, antisense targeting of perlecan blocks tumor growth and angiogenesis in vivo (Aviezer et al., 1997; Sharma et al., 1998).

We do not know whether the abnormal endothelial cell migration and pathfinding is caused by a structural role, abnormal signaling of molecules involved in angiogenesis, or a combination of both. Ultrastructural analysis of vascular, epithelial, and notochord basement membranes revealed no significant abnormalities in the *perlecan* morphants, which is in keeping with the findings of the perlecan-null mouse (Arikawa-Hirasawa et al., 1999; Costell et al., 1999). We favor the possibility that part of the vascular phenotype in the *perlecan* morphants is caused by abnormal signaling events mediated by hedgehog (*hh*) and Vegf proteins and their receptors (Covassin et al., 2006).

Perlecan regulates signaling via protein–protein and protein–carbohydrate interactions (Iozzo, 1998), and recent evidence indicates that perlecan regulates *shh* signaling during development (Park et al., 2003) and cancer (Datta et al., 2006a,b; Lindner et al., 2007). In zebrafish embryos, Hh is secreted by the midline structures (floor plate, notochord, and hypochord) and is at the top of the signaling cascade controlling vasculogenesis, which also includes *vegf* and *notch* (Lawson et al., 2001, 2002). Moreover, Hh is not only required for adult blood stem cell formation and for the expression of artery-specific genes by aortic endothelial cells but is also required for angiogenic sprouting of primary ISV (Gering and Patient, 2005). Interestingly, Hh is essential for endothelial chord and tube formation in avian and murine embryos (Vokes et al., 2004), suggesting that its role in vasculogenesis is conserved in vertebrate embryos. Thus, a plausible scenario is that during somitogenesis and vasculogenesis, Hh activity is perturbed by the lack of perlecan, which might also affect the *vegf–vegfr2* axis as well as other potential players such as the *fgf–fgfr* signaling pathway.

In conclusion, our findings indicate that *perlecan* functions as a key regulator of somitic muscle development and angiogenesis. This study provides new insights into the biology of this important macromolecule and its C-terminal angiostatic fragment endorepellin and predicts the potential existence of human genetic diseases yet to be characterized in which truncated forms of perlecan might directly affect skeletal muscle and vascular development without causing embryonic lethality.

Materials and methods

Zebrafish embryos, *perlecan* morpholino design, and microinjection

Wild-type, Tg*(fli1:egfp)*^{y1} (Lawson and Weinstein, 2002), and Tg*(vegfr2:g-rcfp)* (Cross et al., 2003) zebrafish embryos were maintained according to common practice at ∼28°C in embryo medium. Before 24 hpf, embryo medium was supplemented with phenylthiourea to prevent pigmentation. All embryos were housed in the zebrafish facility of the Kimmel Cancer Center (Thomas Jefferson University) and were cared for/used in accordance with university Institutional Animal Care and Use Committee guidelines. Between 1 and 10 ng of morpholino antisense oligonucleotides or morpholino standard control oligonucleotide was microinjected into one- to two-cell stage embryos as described previously (Nasevicius and Ekker, 2000). Morpholinos (Gene Tools, LLC) were designed to either target the 5′ untranslated region/translation start of zebrafish *perlecan* (MO-DI) or to target a splice junction within *perlecan*'s domain III (MO-DIII) or domain V (MO-DV). *Perlecan* morpholino sequences were as follows: DI-MO, AGTCTTTCAACTCGACCTTCATTCC; DIII-MO, ACGAGTCAACCTGCACAACACACAC; and DV-MO, CATCAAACCTGCAAAAGAAAAATGT. The morpholino standard control oligonucleotide sequence was CCTCTTACCTCAGTTACAATTTATA. Morpholino off-target effects were assessed by coknockdown of p53 with a translation-blocking p53MO, GCGCCATTGCTTTGCAAGAATTG, as previously described (Robu et al., 2007). Gross morphological assessment/phenotypic observations were visualized with a stereomicroscope (MZFIII; Leica) or microscope (Axioplan2; Carl Zeiss, Inc.), which were equipped with a GFP filter set for vascular-specific analysis in the transgenic embryos, and photographed with a camera (Axiocam; Carl Zeiss, Inc.) and AxioVision software version 3.0.6.1 (Carl Zeiss, Inc.). All embryos were mounted in 3–4% methylcellulose on glass slides and anesthetized with Tricaine when necessary.

Live imaging and digital microscopy

DIC and 3D deconvolved GFP images were collected on a fluorescent microscope (DM5500 B; Leica) equipped with a camera (DFC340 FX; Leica) and LAS AF version 1.6.1 (Leica). Live videos with DIC microscopy were captured on the same platform. All video files were exported as AVI files, which were edited in Vegas Movie Studio version 6.0 (Sony) and rendered in QuickTime Pro version 7.0 (Microsoft). All embryos were mounted in 3–4% methylcellulose on glass slides and anesthetized with Tricaine when necessary.

Zebrafish whole mount immunohistochemistry

Zebrafish embryos were fixed in 4% PFA (Thermo Fisher Scientific) in PBS overnight at 4°C. Postfixation embryos were washed three times over 10 min in 1× PBST (PBS + 0.1% Tween 20), and chorions were removed. Embryos were permeabilized by immersion first in distilled H_2O for 5 min followed by immersion in ice-cold acetone at −20°C for 7 min and immersion in distilled H_2O for 5 min. Embryos were rehydrated in decreasing methanol/PBST series (5 min each in 75, 50, and 25%) followed by washing twice over 3 min in PBST. Blocking was performed for a minimum of 4 h by immersing the embryos in a solution of 0.1–0.2% BSA (Sigma-Aldrich) at room temperature. Embryos were incubated with the primary antibody, rabbit anti–mouse perlecan, as previously described (Handler et al., 1997) at a 1:250 dilution in blocking solution overnight at 4°C. Embryos were washed in blocking solution four times over at least 25–30 min. Embryos were incubated with the secondary antibody, donkey anti–rabbit HRP (GE Healthcare), at a 1:1,000 dilution in blocking solution for ∼4 h at room temperature. Embryos were washed in blocking solution four times over at least 25–30 min. Antibody staining was visualized by DAB color development according to the manufacturer's instructions (Dako). Staining reactions were terminated by substrate removal and thorough washing in 1× PBST. Antibody staining was performed on groups of two to five embryos. Embryos incubated with secondary antibody alone served as controls. All embryos were photographed in PBST on an MZFIII stereomicroscope or Axioplan2 microscope with an Axiocam camera and AxioVision software version 3.0.6.1.

Endogenous alkaline phosphatase–based vascular staining

1–3 dpf wild-type embryos were fixed in 4–5% PFA and dehydrated in increasing methanol/PBST series to 100% methanol for storage at −20°C. Embryos were acetone immersed for 30 min at −20°C followed by washing twice for 5 min each in 1× PBST (0.1% Tween 20). Embryos were equilibrated in alkaline phosphatase staining solution three times for 15 min at room temperature (0.1 M Tris-HCl, pH 9.5, 0.1 M NaCl, and 0.05 M $MgCl_2$) and subsequently incubated with the alkaline phosphatase substrates nitroblue tetrazolium chloride/5-bromo-4-chloro-3-indolyl-phosphate, 4-toluidine salt according to the manufacturer's instructions (Roche). Staining reactions were terminated by substrate removal and thorough washing in 1× PBST. Endogenous alkaline phosphatase staining was performed with three embryos per group. Embryos were imaged in PBST with a stereomicroscope (MZ16FA; Leica) equipped with a camera (DFC500; Leica) and Application Suite version 2.5.0 R1 (Leica).

RT-PCR

Zebrafish total RNA (n = 23 embryos per group for morpholino verification experiment; n = 40 embryos per group for developmental analysis) was isolated according to the TRIZOL method (Invitrogen). For reverse transcription, total RNA was annealed with Oligo(dT) primer (Roche) at 70°C for 5 min followed by the addition of 5× Moloney murine leukemia virus buffer (Thermo Fisher Scientific), 10 mM deoxynucleotide triphosphates (Thermo Fisher Scientific), RNAsin (Promega), Moloney murine leukemia virus reverse transcription (Thermo Fisher Scientific), and incubation at 42°C for 1 h. Reverse transcription reactions were heated at 90°C for 10 min followed by incubation at 4°C for 2 min before usage, or reactions were kept at 4°C for prolonged cDNA storage. Perlecan domain III PCR reactions contained cDNA, 10× PCR buffer (Thermo Fisher Scientific), 10 mM deoxynucleotide triphosphates (Thermo Fisher Scientific), 10 pmol/μl DIIIF primer 'GCTAGTGGATCTGTCTCG', and 10 pmol/μl DIIIR primer 'CTCCTCGCTGAAGTGAGT' (Invitrogen). PCR reactions were analyzed on 4% agarose gel electrophoresis.

Zebrafish *endorepellin* riboprobe generation and whole mount ISH

For endorepellin/domain V riboprobe generation, zebrafish *perlecan* domain V sense/antisense riboprobes were synthesized by in vitro transcription from the TOPO (zebrafish domain V) plasmid with Sp6 (Thermo Fisher Scientific) or T7 (Promega) RNA polymerase and were digoxigenin labeled via digoxigenin-UTP (Roche) incorporation during the in vitro transcription reaction. For ISH, RNA localization/detection with sense/antisense riboprobes was performed on groups of two to five embryos essentially as described previously (Childs et al., 2002). All embryos were photographed on an MZFIII stereomicroscope or Axioplan2 microscope with an Axiocam camera and AxioVision software version 3.0.6.1.

Protein rescue

Human perlecan was immunoaffinity purified from the secretions of human coronary arterial endothelial cells using an affinity column containing a monoclonal antibody against perlecan protein core (Whitelock and Iozzo, 2002). Recombinant human endorepellin was purified from 293—Epstein-Barr virus nuclear antigen cells stably transfected with the appropriate vector (Mongiat et al., 2003; Bix et al., 2007). The proteins were diluted to reach a concentration of ∼1 μg/μl, and 2.5–4 nl were microinjected into one- to two-cell stage embryos either alone or in combination with antisense morpholino.

Online supplemental material

Table S1, Table S2, and Fig. S1 show structural analysis of zebrafish *perlecan* and comparative analysis of *Danio rerio* domain V/endorepellin (TPA BK006379 and GenBank/EMBL/DDBJ accession no. EU379567). Fig. S2 shows a comparison of MO-DI and MO-DV perlecan morphants and p53 coknockdown experiments. Fig. S3 shows abnormal skeletal muscle structure at 2 dpf in *perlecan* morphants. Fig. S4 shows protracted *perlecan* knockdown effects on vascular development. Fig. S5 shows vascular analysis in *Tg(fli1:egfp)*^{y1} and *Tg(vegfr2:g-rcfp) perlecan* morphant embryos. Video 1 shows abnormal swimming of *perlecan* morphants, and Videos 2–6 show circulatory analysis through the heart, head, and axial vessels in control and *perlecan* morphant embryos. Online supplemental material is available at http://www.jcb.org/cgi/content/full/jcb.200708022/DC1.

We thank George Purkins for help with the video editing, Bodil Tuma for electron microscopy, Richard L. Rotundo for providing valuable probes, Amy Rubinstein for providing the transgenic *vegfr2–g-rcfp* zebrafish, Peter Yurchenco for providing the antiperlecan antibody, David Birk for use of the Leica microscope, and Shelly Campbell for excellent technical assistance.

This work was supported, in part, by National Institutes of Health grants RO1 CA39481, RO1 CA47282, and RO1 CA120975 (to R.V. Iozzo) and National Institutes of Health National Research Service Award training grant T32 AA07463 (to J.J. Z). This work is a part fulfillment for a doctoral thesis in Cell and Developmental Biology for J.J. Zoeller.

Submitted: 3 August 2007
Accepted: 24 March 2008

References

Arikawa-Hirasawa, E., E. Watanabe, H. Takami, J.R. Hassell, and Y. Yamada. 1999. Perlecan is essential for cartilage and cephalic development. *Nat. Genet.* 23:354–358.

Arikawa-Hirasawa, E., S.G. Rossi, R.L. Rotundo, and Y. Yamada. 2002. Absence of acetylcholinesterase at the neuromuscular junctions of perlecan-null mice. *Nat. Neurosci.* 5:119–123.

Aviezer, D., D. Hecht, M. Safran, M. Eisinger, G. David, and A. Yayon. 1994. Perlecan, basal lamina proteoglycan, promotes basic fibroblast growth factor-receptor binding, mitogenesis, and angiogenesis. *Cell.* 79:1005–1013.

Aviezer, D., R.V. Iozzo, D.M. Noonan, and A. Yayon. 1997. Suppression of autocrine and paracrine functions of basic fibroblast growth factor by stable expression of perlecan antisense cDNA. *Mol. Cell. Biol.* 17:1938–1946.

Bassett, D.I., and P.D. Currie. 2003. The zebrafish as a model for muscular dystrophy and congenital myopathy. *Hum. Mol. Genet.* 12:R265–R270.

Bassett, D.I., R.J. Bryson-Richardson, D.F. Daggett, P. Gautier, D.G. Keenan, and P.D. Currie. 2003. Dystrophin is required for the formation of stable muscle attachments in the zebrafish embryo. *Development.* 130:5851–5860.

Behra, M., X. Cousin, C. Bertrand, J.-L. Vonesch, D. Biellmann, A. Chatonnet, and U. Strähle. 2002. Acetylcholinesterase is required for neuronal and muscular development in the zebrafish embryo. *Nat. Neurosci.* 5:111–118.

Bishop, J.R., M. Schuksz, and J.D. Esko. 2007. Heparan sulphate proteoglycans fine-tune mammalian physiology. *Nature.* 446:1030–1037.

Bix, G., J. Fu, E. Gonzalez, L. Macro, A. Barker, S. Campbell, M.M. Zutter, S.A. Santoro, J.K. Kim, M. Höök, et al. 2004. Endorepellin causes endothelial cell disassembly of actin cytoskeleton and focal adhesions through the α2β1 integrin. *J. Cell Biol.* 166:97–109.

Bix, G., R. Castello, M. Burrows, J.J. Zoeller, M. Weech, R.A. Iozzo, C. Cardi, M.T. Thakur, C.A. Barker, K.C. Camphausen, and R.V. Iozzo. 2006. Endorepellin in vivo: targeting the tumor vasculature and retarding cancer growth and metabolism. *J. Natl. Cancer Inst.* 98:1634–1646.

Bix, G., R.A. Iozzo, B. Woodall, M. Burrows, A. McQuillan, S. Campbell, G.B. Fields, and R.V. Iozzo. 2007. Endorepellin, the C-terminal angiostatic module of perlecan, enhances collagen-platelet responses via the α2β1 integrin receptor. *Blood.* 109:3745–3748.

Carmeliet, P. 2005. Angiogenesis in life, disease and medicine. *Nature.* 438:932–936.

Childs, S., J.-N. Chen, D.M. Garrity, and M.C. Fishman. 2002. Patterning of angiogenesis in the zebrafish embryo. *Development.* 129:973–982.

Costell, M., E. Gustafsson, A. Aszódi, M. Mörgelin, W. Bloch, E. Hunziker, K. Addicks, R. Timpl, and R. Fässler. 1999. Perlecan maintains the integrity of cartilage and some basement membranes. *J. Cell Biol.* 147:1109–1122.

Costell, M., R. Carmona, E. Gustafsson, M. González-Iriarte, R. Fässler, and R. Munoz-Chápuli. 2002. Hyperplastic conotruncal endocardial cushions and transposition of great arteries in perlecan-null mice. *Circ. Res.* 91:158–164.

Covassin, L.D., J.A. Villefranc, M.C. Kacergis, B.M. Weinstein, and N.D. Lawson. 2006. Distinct genetic interactions between multiple Vegf receptors are required for development of different blood vessel types in zebrafish. *Proc. Natl. Acad. Sci. USA.* 103:6554–6559.

Cross, L.M., M.A. Cook, S. Lin, J.-N. Chen, and A.L. Rubinstein. 2003. Rapid analysis of angiogenic drugs in a live fluorescent zebrafish assay. *Arterioscler. Thromb. Vasc. Biol.* 23:911–912.

Datta, M.W., A.M. Hernandez, M.J. Schlicht, A.J. Kahler, A.M. DeGueme, R. Dhir, R.B. Shah, C. Farach-Carson, A. Barrett, and S. Datta. 2006a. *Perlecan*, a candidate gene for the CAPB locus, regulates prostate cancer cell growth via the Sonic Hedgehog pathway. *Mol. Cancer.* 5:9.

Datta, S., M. Pierce, and M.W. Datta. 2006b. Perlecan signaling: helping hedgehog stimulate prostate cancer growth. *Int. J. Biochem. Cell Biol.* 38:1855–1861.

Drapeau, P., R.R. Buss, D.W. Ali, P. Legendre, and R.L. Rotundo. 2001. Limits to the development of fast neuromuscular transmission in zebrafish. *J. Neurophysiol.* 86:2951–2956.

Fuki, I.V., R.V. Iozzo, and K.J. Williams. 2000. Perlecan heparan sulfate proteoglycan. A novel receptor that mediates a distinct pathway for ligand catabolism. *J. Biol. Chem.* 275:25742–25750.

Gering, M., and R. Patient. 2005. Hedgehog signaling is required for adult blood stem cell formation in zebrafish embryos. *Dev. Cell.* 8:389–400.

Gonzalez, E.M., C.C. Reed, G. Bix, J. Fu, Y. Zhang, B. Gopalakrishnan, D.S. Greenspan, and R.V. Iozzo. 2005. BMP-1/Tolloid-like metalloproteases process endorepellin, the angiostatic C-terminal fragment of perlecan. *J. Biol. Chem.* 280:7080–7087.

González-Iriarte, M., R. Carmona, J.M. Pérez-Pomares, D. Macías, M. Costell, and R. Munoz-Chápuli. 2003. Development of the coronary arteries in a murine model of transposition of great arteries. *J. Mol. Cell. Cardiol.* 35:795–802.

Granato, M., F.J.M. van Eeden, U. Schach, T. Trowe, M. Brand, M. Furutani-Seiki, P. Haffter, M. Hammerschmidt, C.-P. Heisenberg, Y.-J. Jiang, et al. 1996. Genes controlling and mediating locomotion behavior of the zebrafish embryo and larva. *Development.* 123:399–413.

Guyon, J.R., A.N. Mosley, S.J. Jun, F. Montanaro, L.S. Steffen, Y. Zhou, V. Nigro, L.I. Zon, and L.M. Kunkel. 2005. δ-sarcoglycan is required for early zebrafish muscle organization. *Exp. Cell Res.* 304:105–115.

Guyon, J.R., L.S. Steffen, M.H. Howell, T.J. Pusack, C. Lawrence, and L.M. Kunkel. 2007. Modeling human muscle disease in zebrafish. *Biochim. Biophys. Acta.* 1772:205–215.

Handler, M., P.D. Yurchenco, and R.V. Iozzo. 1997. Developmental expression of perlecan during murine embryogenesis. *Dev. Dyn.* 210:130–145.

Hassell, J, Y. Yamada, and E. Arikawa-Hirasawa. 2002. Role of perlecan in skeletal development and diseases. *Glycoconj. J.* 19:263–267.

Iozzo, R.V. 1998. Matrix proteoglycans: from molecular design to cellular function. *Annu. Rev. Biochem.* 67:609–652.

Iozzo, R.V. 2005. Basement membrane proteoglycans: from cellar to ceiling. *Nat. Rev. Mol. Cell Biol.* 6:646–656.

Iozzo, R.V., and J.D. San Antonio. 2001. Heparan sulfate proteoglycans: heavy hitters in the angiogenesis arena. *J. Clin. Invest.* 108:349–355.

Isogai, S., M. Horiguchi, and B.M. Weinstein. 2001. The vascular anatomy of the developing zebrafish: an atlas of embryonic and early larval development. *Dev. Biol.* 230:278–301.

Isogai, S., N.D. Lawson, S. Torrealday, M. Horiguchi, and B.M. Weinstein. 2003. Angiogenic network formation in the developing vertebrate trunk. *Development.* 130:5281–5290.

Kanagawa, M., D.E. Michele, J.S. Satz, R. Barresi, H. Kusano, T. Sasaki, R. Timpl, M.D. Henry, and K.P. Campbell. 2005. Disruption of perlecan binding and matrix assembly by post-translational or genetic disruption of dystroglycan function. *FEBS Lett.* 579:4792–4796.

Knox, S.M., and J.M. Whitelock. 2006. Perlecan: how does one molecule do so many things? *Cell. Mol. Life Sci.* 63:2435–2445.

Kunkel, L.M., E. Bachrach, R.R. Bennett, J. Guyon, and L. Steffen. 2006. Diagnosis and cell-based therapy for duchenne muscular dystrophy in humans, mice, and zebrafish. *J. Hum. Genet.* 51:397–406.

Lawson, N.D., and B.M. Weinstein. 2002. *In vivo* imaging of embryonic vascular development using transgenic zebrafish. *Dev. Biol.* 248:307–318.

Lawson, N.D., N. Scheer, V.N. Pham, C.-H. Kim, A.B. Chitnis, J.A. Campos-Ortega, and B.M. Weinstein. 2001. Notch signaling is required for arterial-venous differentiation during embryonic vascular development. *Development.* 128:3675–3683.

Lawson, N.D., A.M. Vogel, and B.M. Weinstein. 2002. *sonic hedgehog* and *vascular endothelial growth factor* act upstream of the Notch pathway during arterial endothelial differentiation. *Dev. Cell.* 3:127–136.

Lindner, J.R., P.R. Hillman, A.L. Barrett, M.C. Jackson, T.L. Perry, Y. Park, and S. Datta. 2007. The *Drosophila* Perlecan gene *trol* regulates multiple signaling pathways in different developmental contexts. *BMC Dev. Biol.* 7:121.

Mathiak, M., C. Yenisey, D.S. Grant, B. Sharma, and R.V. Iozzo. 1997. A role for perlecan in the suppression of growth and invasion in fibrosarcoma cells. *Cancer Res.* 57:2130–2136.

Mongiat, M., S. Sweeney, J.D. San Antonio, J. Fu, and R.V. Iozzo. 2003. Endorepellin, a novel inhibitor of angiogenesis derived from the C terminus of perlecan. *J. Biol. Chem.* 278:4238–4249.

Nasevicius, A., and S.C. Ekker. 2000. Effective targeted gene 'knockdown' in zebrafish. *Nat. Genet.* 26:216–220.

Nasevicius, A., J. Larson, and S.C. Ekker. 2000. Distinct requirements for zebrafish angiogenesis revealed by a *VEGF-A* morphant. *Yeast.* 17:294–301.

Park, Y., C. Rangel, M.M. Reynolds, M.C. Caldwell, M. Johns, M. Nayak, C.J.R. Welsh, S. McDermott, and S. Datta. 2003. *Drosophila* perlecan modulates FGF and hedgehog signals to activate neural stem cell division. *Dev. Biol.* 253:247–257.

Parsons, M.J., I. Campos, E.M.A. Hirst, and D.L. Stemple. 2002. Removal of dystroglycan causes severe muscular dystrophy in zebrafish embryos. *Development.* 129:3505–3512.

Peng, H.B., A.A. Ali, D.F. Daggett, H. Rauvala, J.R. Hassell, and N.R. Smalheiser. 1998. The relationship between perlecan and dystroglycan and its implication in the formation of the neuromuscular junction. *Cell Adhes. Commun.* 5:475–489.

Peng, H.B., H. Xie, S.G. Rossi, and R.L. Rotundo. 1999. Acetylcholinesterase clustering at the neuromuscular junction involves perlecan and dystroglycan. *J. Cell Biol.* 145:911–921.

Robu, M.E., J.D. Larson, A. Nasevicius, S. Beiraghi, C. Brenner, S.A. Farber, and S.C. Ekker. 2007. p53 activation by knockdown technologies. *PLoS Genet.* 3:e78.

Rodgers, K.D., T. Sasaki, A. Aszodi, and O. Jacenko. 2007. Reduced perlecan in mice results in chondrodysplasia resembling Schwartz-Jampel syndrome. *Hum. Mol. Genet.* 16:515–528.

Rossi, M., H. Morita, R. Sormunen, S. Airenne, M. Kreivi, L. Wang, N. Fukai, B.R. Olsen, K. Tryggvason, and R. Soininen. 2003. Heparan sulfate chains of perlecan are indispensable in the lens capsule but not in the kidney. *EMBO J.* 22:236–245.

Rotundo, R.L. 2003. Expression and localization of acetylcholinesterase at the neuromuscular junction. *J. Neurocytol.* 32:743–766.

Schneider, M., A.A. Khalil, J. Poulton, C. Castillejo-Lopez, D. Egger-Adam, A. Wodarz, W.-M. Deng, and S. Baumgartner. 2006. Perlecan and dystroglycan act at the basal side of the *Drosophila* follicular epithelium to maintain epithelial organization. *Development.* 133:3805–3815.

Sharma, B., M. Handler, I. Eichstetter, J. Whitelock, M.A. Nugent, and R.V. Iozzo. 1998. Antisense targeting of perlecan blocks tumor growth and angiogenesis in vivo. *J. Clin. Invest.* 102:1599–1608.

Smirnov, S.P., P. Barzaghi, K.K. McKee, M.A. Ruegg, and P.D. Yurchenco. 2005. Conjugation of LG domains of agrins and perlecan to polymerizing laminin-2 promotes acetylcholine receptor clustering. *J. Biol. Chem.* 280:41449–41457.

Stum, M., C.-S. Davoine, S. Vicart, L. Guillot-Noël, H. Topaloglu, F.J. Carod-Artal, H. Kayserili, F. Hentati, L. Merlini, J.A. Urtizberea, et al. 2006. Spectrum of *HSPG2* (perlecan) mutations in patients with schwartz-jampel syndrome. *Hum. Mutat.* 27:1082–1091.

Talts, J.F., Z. Andac, W. Göhring, A. Brancaccio, and R. Timpl. 1999. Binding of the G domains of laminin α1 and α2 chains and perlecan to heparin, sulfatides, α-dystroglycan and several extracellular matrix proteins. *EMBO J.* 18:863–870.

Tran, P.-K., K. Tran-Lundmark, R. Soininen, K. Tryggvason, J. Thyberg, and U. Hedin. 2004. Increased intimal hyperplasia and smooth muscle cell proliferation in transgenic mice with heparan sulfate-deficient perlecan. *Circ. Res.* 94:550–558.

Villar, M.J., J.R. Hassell, and E. Brandan. 1999. Interaction of skeletal muscle cells with collagen type IV is mediated by perlecan associated with the cell surface. *J. Cell. Biochem.* 75:665–674.

Vokes, S.A., T.A. Yatskievych, R.L. Heimark, J. McMahon, A.P. McMahon, P.B. Antin, and P.A. Krieg. 2004. Hedgehog signaling is essential for endothelial tube formation during vasculogenesis. *Development.* 131:4371–4380.

Wang, H., K. Julenius, J. Hryhorenko, and F.K. Hagen. 2007. Systematic analysis of proteoglycan modification sites in *Caenorhabditis elegans* by scanning mutagenesis. *J. Biol. Chem.* 282:14586–14597.

Whitelock, J.M., and R.V. Iozzo. 2002. Isolation and purification of proteoglycans. *In* Methods in Cell-Matrix Adhesion. J.C. Adams, editor. Academic Press, San Diego. 53–67.

Whitelock, J.M., and R.V. Iozzo. 2005. Heparan sulfate: a complex polymer charged with biological activity. *Chem. Rev.* 105:2745–2764.

Whitelock, J.M., L.D. Graham, J. Melrose, A.D. Murdoch, R.V. Iozzo, and P.A. Underwood. 1999. Human perlecan immunopurified from different endothelial cell sources has different adhesive properties for vascular cells. *Matrix Biol.* 18:163–178.

Woodall, B.P., A. Nyström, R.A. Iozzo, J.A. Eble, S. Niland, T. Krieg, B. Eckes, A. Pozzi, and R.V. Iozzo. 2008. Integrin α2β1 is the required receptor for endorepellin angiostatic activity. *J. Biol. Chem.* 283:2335–2343.

Zhou, Z., J. Wang, R. Cao, H. Morita, R. Soininen, K.M. Chan, B. Liu, Y. Cao, and K. Tryggvason. 2004. Impaired angiogenesis, delayed wound healing and retarded tumor growth in perlecan heparan sulfate-deficient mice. *Cancer Res.* 64:4699–4702.

Zoeller, J.J., and R.V. Iozzo. 2008. Proteomic profiling of endorepellin angiostatic activity on human endothelial cells. *Proteome Sci.* 6:7.